Research Article | Vol. 25, No. 3 | 6 Feb 2017 | OPTICS EXPRESS 2195

Optics EXPRESS

Axial beam scanning in multiphoton microscopy with MEMS-based actuator

XIYU DUAN,[1] HAIJUN LI,[2] XUE LI,[2] KENN R. OLDHAM,[3] AND THOMAS D. WANG[1,2,3,*]

[1]*Dept. of Biomedical Engineering, University of Michigan, Ann Arbor, MI, USA*
[2]*Dept. of Internal Medicine, Division of Gastroenterology, University of Michigan, Ann Arbor, MI, USA*
[3]*Dept. of Mechanical Engineering, University of Michigan, Ann Arbor, MI, USA*
[*]*thomaswa@umich.edu*

Abstract: We demonstrate a remotely located microelectromechanical systems (MEMS) actuator that can translate >400 μm to perform axial beam scanning in a multiphoton microscope. We use a 2-dimensional MEMS mirror for lateral scanning, and collected multiphoton excited fluorescence images in either the horizontal or vertical plane with a field-of-view of either 270 × 270 or 270 × 200 μm^2, respectively, at 5 frames per second. Axial resolution varied from 4.5 to 7 μm over the scan range. The compact size of the actuator and scanner allows for use in an endomicroscope to collect images in the vertical plane with >200 μm depth.

OCIS codes: (190.4180) Multiphoton processes; (230.4040) Mirrors.

References and links

1. W. Denk, J. H. Strickler, and W. W. Webb, "Two-photon laser scanning fluorescence microscopy," Science **248**(4951), 73–76 (1990).
2. A. Masedunskas, M. Sramkova, L. Parente, and R. Weigert, "Intravital Microscopy to Image Membrane Trafficking in Live Rats," Methods Mol. Biol. **931**, 153–167 (2012).
3. L. Ritsma, E. J. A. Steller, E. Beerling, C. J. M. Loomans, A. Zomer, C. Gerlach, N. Vrisekoop, D. Seinstra, L. van Gurp, R. Schafer, D. A. Raats, A. de Graaff, T. N. Schumacher, E. J. P. de Koning, O. Kranenburg, and J. van Rheenen, "Intravital Microscopy through an Abdominal Imaging Window Reveals Steps during Liver Metastasis," Sci. Transl. Med. **4**(158), 158ra145 (2012).
4. E. K. Griffiths, O. Sanchez, P. Mill, C. Krawczyk, C. V. Hojilla, E. Rubin, M. M. Nau, R. Khokha, S. Lipkowitz, C. C. Hui, and J. M. Penninger, "Cbl-3-deficient mice exhibit normal epithelial development," Mol. Cell. Biol. **23**(21), 7708–7718 (2003).
5. H. Clevers, "The intestinal crypt, a prototype stem cell compartment," Cell **154**(2), 274–284 (2013).
6. M. J. Koehler, T. Vogel, P. Elsner, K. König, R. Bückle, and M. Kaatz, "In vivo measurement of the human epidermal thickness in different localizations by multiphoton laser tomography," Skin Res. Technol. **16**(3), 259–264 (2010).
7. W. Göbel, F. Helmchen, and B. M. Kampa, "Imaging cellular network dynamics in three dimensions using fast 3D laser scanning," Nat. Methods **4**(1), 73–79 (2007).
8. S. J. Miller, B. P. Joshi, A. Gaustad, Y. Feng, E. R. Fearon, and T. D. Wang, "In vivo Fluorescence-Based Endoscopic Detection of Colon Dysplasia in the Mouse using a Novel Peptide Probe," PLoS one **6**(3), e17384 (2011).
9. E. J. Botcherby, C. W. Smith, M. M. Kohl, D. Débarre, M. J. Booth, R. Juškaitis, O. Paulsen, and T. Wilson, "Aberration-free three-dimensional multiphoton imaging of neuronal activity at kHz rates," Proc. Natl. Acad. Sci. U.S.A. **109**(8), 2919–2924 (2012).
10. E. J. Botcherby, R. Juskaitis, M. J. Booth, and T. Wilson, "Aberration-free optical refocusing in high numerical aperture microscopy," Opt. Lett. **32**(14), 2007–2009 (2007).
11. W. Piyawattanametha, R. P. Barretto, T. H. Ko, B. A. Flusberg, E. D. Cocker, H. Ra, D. Lee, O. Solgaard, and M. J. Schnitzer, "Fast-scanning two-photon fluorescence imaging based on a microelectromechanical systems two- dimensional scanning mirror," Opt. Lett. **31**(13), 2018–2020 (2006).
12. W. Piyawattanametha, E. D. Cocker, R. P. Barretto, J. C. Jung, H. Ra, O. Solgaard, and M. J. Schnitzer, "Fast-scanning two-photon fluorescence imaging based on a microelectromechanical systems two- dimensional scanning mirror," Opt. Lett. **34**(15), 2309–2311 (2009).
13. K. Lee, K. Krisnamoorthy, K. Yu, and O. Solgaard, "Single-crystalline silicon micromirrors actuated by self-aligned vertical electrostatic comb drives with piston-motion and rotational capabilities," Sens. Actuators A Phys. **114**(2–3), 423–428 (2004).

#281216 https://doi.org/10.1364/OE.25.002195
Journal © 2017 Received 21 Nov 2016; revised 20 Jan 2017; accepted 21 Jan 2017; published 26 Jan 2017

Optics EXPRESS

14. L. Fu, A. Jain, C. Cranfield, H. Xie, and M. Gu, "Three-dimensional nonlinear optical endoscopy," J. Biomed. Opt. **12**(4), 040501 (2007).
15. Y. Zhu, W. Liu, K. Jia, W. Liao, and H. Xie, "A piezoelectric unimorph actuator based tip-tilt-piston micromirror with high fill factor and small tilt and lateral shift," Sens. Actuators **167**(2), 495–501 (2011).
16. H. Mansoor, H. Zeng, K. Chen, Y. Yu, J. Zhao, and M. Chiao, "Vertical optical sectioning using a magnetically driven confocal microscanner aimed for in vivo clinical imaging," Opt. Express **19**(25), 25161–25172 (2011).
17. E. E. Hoover, M. D. Young, E. V. Chandler, A. Luo, J. J. Field, K. E. Sheetz, A. W. Sylvester, and J. A. Squier, "Remote focusing for programmable multi-layer differential multiphoton microscopy," Biomed. Opt. Express **2**(1), 113–122 (2011).
18. P. Rupprecht, A. Prendergast, C. Wyart, and R. W. Friedrich, "Remote z-scanning with a macroscopic voice coil motor for fast 3D multiphoton laser scanning microscopy," Biomed. Opt. Express **7**(5), 1656–1671 (2016).
19. D. R. Rivera, C. M. Brown, D. G. Ouzounov, W. W. Webb, and C. Xu, "Multifocal multiphoton endoscope," Opt. Lett. **37**(8), 1349–1351 (2012).
20. Y. Wu, Y. Zhang, J. Xi, M.-J. Li, and X. Li, "Fiber-optic nonlinear endomicroscopy with focus scanning by using shape memory alloy actuation," J. Biomed. Opt. **15**(6), 060506 (2010).
21. H. Li, X. Duan, Z. Qiu, Q. Zhou, K. Kurabayashi, K. R. Oldham, and T. D. Wang, "Integrated monolithic 3D MEMS scanner for switchable real time vertical/horizontal cross-sectional imaging," Opt. Express **24**(3), 2145–2155 (2016).
22. K. L. Turner, S. A. Miller, P. G. Hartwell, N. C. MacDonald, S. H. Strogatz, and S. G. Adams, "Five parametric resonances in a microelectromechanical system," Nature **396**(6707), 149–152 (1998).
23. A. D. Rakić, "Algorithm for the determination of intrinsic optical constants of metal films: application to aluminum," Appl. Opt. **34**(22), 4755–4767 (1995).
24. M. Drobizhev, N. S. Makarov, S. E. Tillo, T. E. Hughes, and A. Rebane, "Two-photon absorption properties of fluorescent proteins," Nat. Methods **8**(5), 393–399 (2011).
25. L. Madisen, T. A. Zwingman, S. M. Sunkin, S. W. Oh, H. A. Zariwala, H. Gu, L. L. Ng, R. D. Palmiter, M. J. Hawrylycz, A. R. Jones, E. S. Lein, and H. Zeng, "A robust and high-throughput Cre reporting and characterization system for the whole mouse brain," Nat. Neurosci. **13**(1), 133–140 (2010).
26. T. Hinoi, M. Loda, and E. R. Fearon, "Silencing of CDX2 expression in colon cancer via a dominant repression pathway," J. Biol. Chem. **278**(45), 44608–44616 (2003).
27. A. D. Corbett, R. A. B. Burton, G. Bub, P. S. Salter, S. Tuohy, M. J. Booth, and T. Wilson, "Quantifying distortions in two-photon remote focussing microscope images using a volumetric calibration specimen," Front. Physiol. **5**, 384 (2014).
28. G. Ducourthial, P. Leclerc, T. Mansuryan, M. Fabert, J. Brevier, R. Habert, F. Braud, R. Batrin, C. Vever-Bizet, G. Bourg-Heckly, L. Thiberville, A. Druilhe, A. Kudlinski, and F. Louradour, "Development of a real-time flexible multiphoton microendoscope for label-free imaging in a live animal," Sci. Rep. **5**, 18303 (2015).
29. C. J. Engelbrecht, R. S. Johnston, E. J. Seibel, and F. Helmchen, "Ultra-compact fiber-optic two-photon microscope for functional fluorescence imaging in vivo," Opt. Express **16**(8), 5556–5564 (2008).

1. Introduction

Multiphoton microscopy uses near-infrared excitation to minimize tissue scattering and absorption and to reduce background [1]. This technique produces deep tissue penetration with reduced phototoxicity. However, imaging in 3-dimensions (3D) has not been fully developed in vivo. Images in the horizontal (XY) plane can be collected easily using 2-dimensional lateral beam scanning. However, images in the vertical (XZ) plane proven difficult to collect because either the objective or specimen must physically move. This view is often obtained by collecting a Z-stack of horizontal images followed by an image reconstruction but is time-consuming and prone to motion artifacts from vibrations from specimen movement. In vivo imaging in small animals with bulk objectives requires wide surgical exposure that results in terminal experiments [2]. Abdominal windows have been implanted over tumors for longitudinal imaging studies that reduce working distance and are prone to breaking [3].

Many important biological processes, such as normal epithelial development [4], stem cell migration [5], wound healing [6], and neuronal activity [7], require images collected in the vertical plane to be properly studied. The epithelium of hollow organs, such as colon, is a thin layer of metabolically active tissue with depth of ~200 μm in small animals, such as mice [8]. These processes can be observed in vivo if a sufficiently small scanning mechanism can be developed. Imaging in the vertical plane with beam scanning has been performed using a remotely located galvo mirror. Two high numerical aperture objectives are used that introduce equal but opposite aberrations in the excitation wavefront during scanning [9,10].

Optics EXPRESS

Images are collected at fast scan speeds with minimal distortion. However, this approach is bulky and cannot be conducted without surgically altering the animal, thus repetitive imaging needed to track biological behavior cannot be performed.

Previously, lateral beam scanning has been demonstrated in a multiphoton endomicroscope using tiny mirrors developed with microelectromechanical systems (MEMS) fabrication methods [11]. However, images were collected in the horizontal (XY) plane only. A slow micromotor was used to adjust the axial position, and the images were prone to motion artifact [12]. Other electrostatic MEMS scanners have been developed but with small axial displacements that are inadequate to visualize the full depth of the epithelium [13]. Electrothermal devices can provide large axial displacements at low voltages but at slow speeds [14]. Piezoelectric scanners can achieve large axial displacements, but have high fabrication complexity [15]. Electromagnetic scanners have been developed with fast response times and good displacement, but this technology is difficult to scale down in size [16].

Other mechanisms have been made to integrate axial actuators in remote scan configurations. A commercial piezoelectric motor was used to move a mirror [17], but the scan speed was not reported. A fast moving mirror was constructed using a pair of identical galvo motors mounted in opposite directions with scan rate up to 2.7 kHz [9]. The scan performance was excellent and well characterized, and feedback control was used. However, this approach is too bulky for use in an endomicroscope. A voice coil motor has been used for axial scanning at a rate of ~100 Hz [18]. However, a separate sensor and controller was needed to control motion from position drifts, and the size of the actuator was too large to miniaturize the instrument. Adjustment of depth focus has been demonstrated by using three axially offset optical fibers [19], and using a shape memory alloys to move the fiber position [20].

We have developed a lateral MEMS scanner for multiphoton endomicroscopy using the principle of parametric resonance [21], where the drive signal is applied at frequencies near $2\omega_o/n$ (ω_o is the natural frequency of vibrational modes and n is an integer ≥1) [22]. Here, we aim to demonstrate a compact MEMS actuator that performs axial beam scanning to collect multiphoton excited fluorescence images in the vertical plane.

2. Methods

2.1 Experimental setup

A Ti-sapphire (Mai Tai DeepSee HP DS, Spectra-Physics) laser with a tunable spectral range of 690-1040 nm provides excitation (red arrows) with ~100 fs pulse width at 80 MHz, Fig. 1(a). The pulse duration was minimized with a dispersion pre-compensation unit located inside the laser housing. A half wave plate (HWP, 10RP42-3, Newport) is used in combination with a linear polarizer (LP, 10GL08AR.16, Newport) to adjust power. The beam is initially p-polarized after passing through a polarizing beam splitter (PBS, PBS252, Thorlabs). After passing through a quarter wave plate (QWP, WPQ10M-780, Thorlabs), reflecting off the lateral scanning MEMS mirror M_1, and passing back through the QWP, the beam becomes s-polarized.

After reflecting off the PBS at 90°, the excitation beam is expanded by a pair of lenses, L_1 (f = 35 mm, LA1951-B, Thorlabs) and L_2 (f = 100 mm, LA1509-B, Thorlabs) to fill the back aperture of the first objective Obj_1 (NA = 0.4, PLN 20X, Olympus). A second PBS reflects the beam through a QWP onto the axial MEMS mirror M_2. The wavefront passes back through the QWP and PBS. The beam is expanded by a pair of telescope lenses L_3 and L_4 (f = 75 mm, LA1608-B, Thorlabs), reflects off a dichroic mirror (DM, 650DCSPXR, Chroma) at 90°, and fills the back aperture of Obj_2 (NA = 0.9, LUMPlanFL/IR 60X/0.9w, Olympus), a water immersion lens. Translation of M_2 results in axial displacement of the focus below the tissue surface with a magnification of ~2:1. Multiphoton excited fluorescence (green arrows)

Optics EXPRESS

generated from the specimen passes through DM, reflects off the planar mirror (M_3, PF10-03-F01, Thorlabs), and is focused by L_5 (f = 60 mm, LA1134-A, Thorlabs) and L_6 (f = 35 mm, LA1951-B, Thorlabs) through a band pass filter (BPF, FGB39, Thorlabs) that has ~80% transmission from 380 to 580 nm onto a photomultiplier tube (PMT, H7422-40, Hamamatsu) detector.

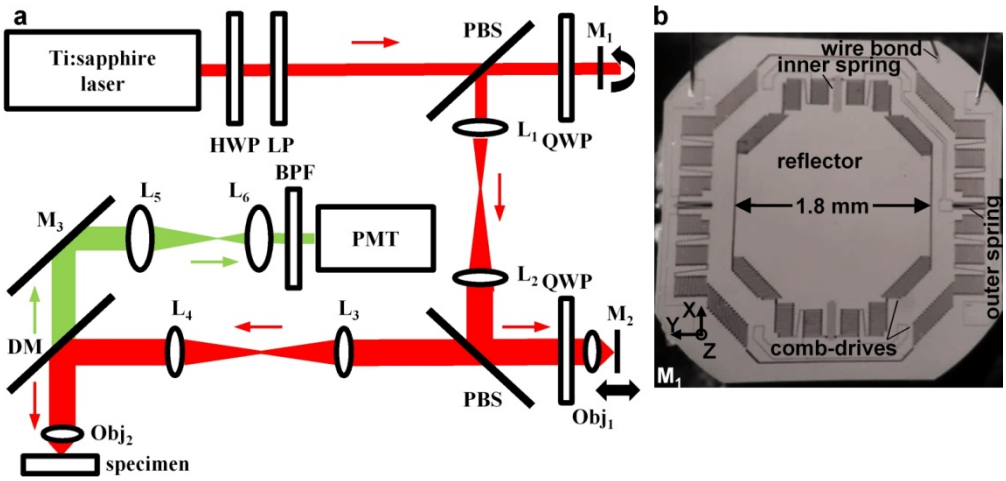

Fig. 1. (a) Schematic of multiphoton microscope. Compact, lightweight MEMS mirrors M_1 and M_2 are located remotely and used for lateral scanning and axial actuation, respectively. The mirrors translate the excitation wavefront between two objectives (Obj_1 and Obj_2) that introduce equal but opposite aberrations to produce axial scanning below the surface of the specimen. Key: HWP: half wave plate, LP: linear polarizer, PBS: polarizing beam splitter, QWP: quarter wave plate, $L_{1\text{-}6}$: lenses, $Obj_{1,2}$: objectives, $M_{1\text{-}3}$: mirrors, DM: dichroic mirror, BPF: bandpass filter, PMT: photomultiplier tube. (b) Lateral MEMS scanner. Compact 2D device has a chip size of 3 × 3 mm^2. The aluminum (Al) coated reflector has dimensions of 1.8 mm, and is mounted on a gimbal frame. Orthogonal electrostatic comb-drive actuators are coupled to inner and outer torsional springs to produce rapid Lissajous scanning.

The PMT signal is amplified by a high-speed current amplifier (59-178, Edmund Optics). We used high-speed data acquisition boards to digitize the fluorescence signal from the PMT (National Instruments, PCI-6115) and to generate control signals to drive the two MEMS scanners (National Instruments, PCI-6711). A personal computer running custom LabVIEW software was used to control and synchronize the boards. By actuating different axes of the MEMS scanners, we were able to switch the scan direction between the horizontal (XY) and vertical (XZ) planes.

2.2 Lateral MEMS scanner

We have previously developed a 2-dimensional (2D) electrostatic MEMS scanner that performs wide lateral deflection [21]. We now modify our previous design by increasing the resonance frequency to scan at higher frame rates. We designed the lateral dimension of the mirror to accommodate the 1.8 mm width of the excitation beam at normal incidence, Fig. 1(b). The mirror is mounted onto a gimbal frame to minimize cross-talk between the X (inner) and Y (outer) axes. Orthogonal sets of electrostatic comb-drive actuators are coupled to inner and outer torsional springs that are designed to achieve resonance. On the front-side of the device, we deposited a 70 nm layer of aluminum (Al) to achieve >85% reflectivity between 200 and 900 nm to reflect a range of wavelengths for multiphoton excitation [23].

2.3 Axial MEMS scanner

We developed a 1-dimensional (1D) electrostatic MEMS actuator that produces >400 μm of out-of-plane (axial) translation along the optical axis to create images in the plane

Optics EXPRESS

perpendicular to tissue surface (vertical) with >200 μm displacement below. We attached two sets of U-shaped levers via serpentine springs to the top and bottom of a 2 mm diameter circular reflector. We placed four columns of electrostatic comb-drive actuators on either side of the reflector to produce a large driving force to activate the levers. By rotating the levers in-phase, the reflector is displaced out-of-plane. On the other hand, by rotating the levers out-of-phase, the reflector deflects about the Y axis instead. We designed the resonance frequency to be ~500 Hz for vertical motion. The mirror surface was also coated with aluminum (Al) for high reflectivity for multiphoton excitation. We used a displacement sensor to measure the movement of the mirror surface and to characterize the frequency response. Scanner performance was characterized by sweeping the drive frequency applied to the actuator at various voltages and duty cycles using either an upsweep (low-to-high) or downsweep (high-to-low) in frequency.

2.4 Performance of remote axial scan

To image in the horizontal (XY) plane, we actuate both the inner and outer axes of the lateral MEMS scanner M_1. We designed the resonant frequencies of these axes to be ~1 and ~4 kHz, respectively. Also, we combine actuation of the inner axis of the lateral scanner with the out-of-plane motion of the axial actuator to image in the vertical (XZ) plane. We developed custom software in LabVIEW (National Instruments) to synchronize the drive signals to the MEMS scanner and actuator. We reconstruct images in the vertical plane by remapping the time series signal to a 2D image using calibrated motion profiles from the scanner and generated lookup tables (LUT). We quantified the relationship between the axial displacement of M_2 and the focus by mounting both the MEMS actuator and specimen stage on motorized stages (TRA12CC, Newport). We moved M_2 to different positions, and measured the corresponding change in location of focus. We quantified the full-width-at-half-maximum (FWHM) to evaluate axial resolution of the system by measuring the response to a 0.1 um fluorescent beads sample translated in either direction about the neutral position located at a working distance of 100 μm in scatter-free air film.

2.5 Imaging of epithelium

We collected multiphoton excited fluorescence images of pollen (Carolina Biological Supply Inc) with dimensions ranging from 30 to 40 μm to demonstrate optical sectioning with axial beam scanning. Using excitation at λ_{ex} = 850 nm, we collected autofluorescence from the grains. A Z-stack of horizontal (XY) images was collected by moving the specimen in the axial direction at 1 μm increments. 3D volumetric images were reconstructed, and the projection in the XZ plane was produced using custom software. We also collected multiphoton excited fluorescence images in the XZ plane directly by translating the axial MEMS actuator M_2 for comparison.

Animal studies were performed in compliance with all University of Michigan regulations and with approval by the University Committee on the Use and Care of Animals (UCUCA). We used a genetically engineered mouse that expresses tdTomato. This optical reporter has peak multiphoton absorbance at ~700 nm [24]. In the wild-type (wt) mouse, a *loxP*-flanked STOP cassette prevents transcription of the downstream tdTomato gene. When bred with mice that express Cre recombinase under control of the human *CDX2* promoter/enhancer sequence (CPC), the STOP cassette is deleted [25], and tdTomato is expressed constitutively in the epithelium of adult mouse colon [26]. For imaging experiments, mice were euthanized. The colon was excised, divided longitudinally, rinsed with PBS to remove debris, and mounted on a glass slide. We used multiphoton excitation at λ_{ex} = 750 nm with ~20 mW of laser power incident on the mucosa to collect fluorescence images.

Optics EXPRESS

3. Results

3.1 Lateral MEMS scanner

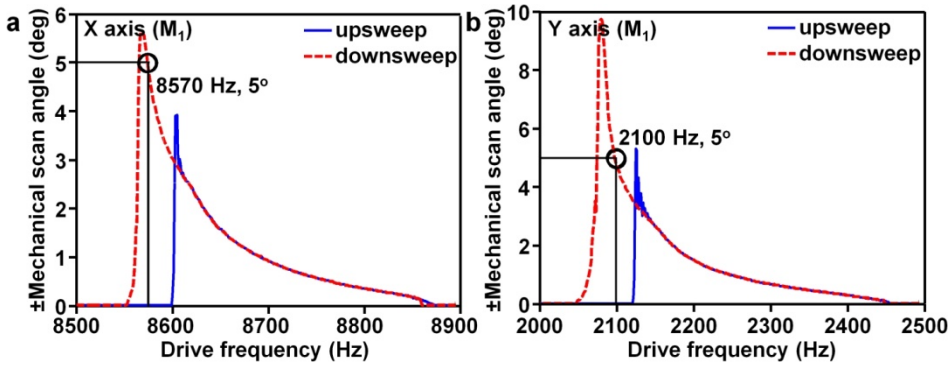

Fig. 2. Performance of lateral MEMS scanner. Frequency response shows mechanical scan angles ≥5° for the (a) inner (X) and (b) outer (Y) axes. For imaging, we applied a sine wave at 60 V_{pp} in a downsweep (red) at drive frequencies of 8570 and 2100 Hz, respectively. The non-linear response of the scanner results from complex interactions in the springs, including electrostatic softening, mechanical hardening, and structural damping.

The compact lateral MEMS scanner M_1 was fabricated with an overall chip size of 3 × 3 mm^2, and the width of the reflector is 1.8 mm, Fig. 1(b). We measured the angular deflection of the lateral MEMS scanner in either axis, Fig. 2(a), 2(b). The frequency response of the scanner to a sine-wave drive signal at 60 V_{pp} for rotation about the X and Y axes is shown. Large scan angles can be achieved with either a downsweep (red) or an upsweep (blue). We found greater deflection angles with a downsweep, and achieved >5° mechanical scan angle in both the X and Y axes. We used drive frequencies of 8570 Hz and 2100 Hz to produce actual tilt frequencies of 4285 Hz and 1050 Hz in the X and Y axes, respectively, from the parametric resonance effect. Lateral scanning about the X and Y axes forms a dense Lissajous pattern that repeats itself at 5 frames per sec to create an image with dimensions of 400 × 400 pixels at 100% coverage.

3.2 Axial MEMS scanner

The compact axial MEMS actuator M_2 was fabricated with a slightly larger chip size of 3.7 × 3.2 mm^2 and a reflector with diameter of 2 mm, Fig. 3(a). The frequency response was characterized by sweeping the drive frequency between 870 Hz and 1000 Hz using a 60 V_{pp} square wave with 30% duty cycle, Fig. 3(b). Unlike the lateral MEMS scanner, this device has a larger displacement during an upsweep (blue) versus downsweep (red). For imaging, we can achieve displacements of >400 μm at a drive frequency of 930 Hz, resulting in actuation at 465 Hz from the parametric resonance effect.

Optics EXPRESS

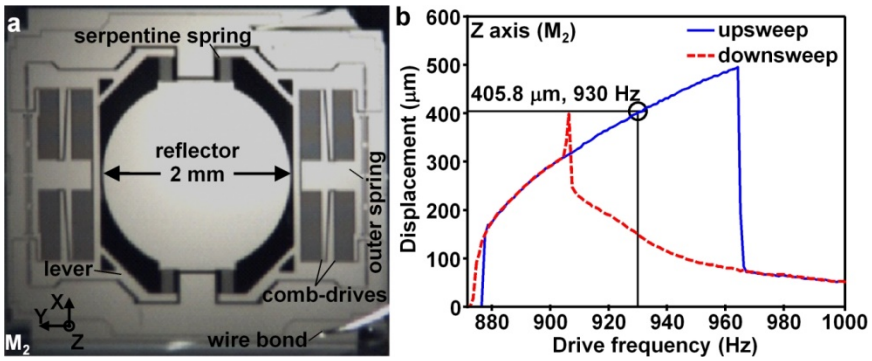

Fig. 3. Axial MEMS actuator. (a) Compact device has a 2 mm diameter circular reflector actuated by two sets of U-shaped levers coupled to serpentine springs to produce large out-of-plane displacement when driven in phase. (b) For imaging, we applied a square wave at 60 V_{pp} in an upsweep (blue) at a drive frequency of 930 Hz to achieve vertical displacement >400 µm.

We observed large differences in mirror deflection amplitude for upsweep versus downsweep that may be caused by a softening effect in the springs. Electrostatic forces at greater distances from the static mirror position are reduced, resulting in a dynamic bifurcation with two stable modes. One occurs at the origin and the other is found at the stable limit cycle that produces large deflections. In practice, the largest deflections are observed when approached from higher frequencies (downsweep) because of a gradual increase in oscillation amplitude from the softening resonant peak being tilted in this direction. Approached from lower frequencies, the origin remains at the stable bifurcation branch until the point where the upsweep and downsweep responses converge. We observed the opposite effect for the axial actuator.

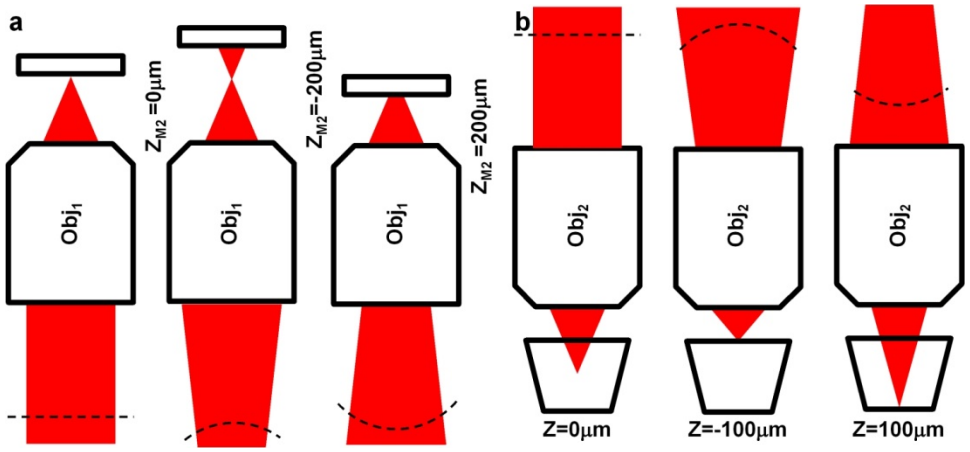

Fig. 4. Axial scan. In the neutral position, the multiphoton excitation wavefront is imaged onto the focal plane at position Z = 0 µm, defined at a distance of 100 µm below the mucosal surface. (a) When the axial MEMS actuator M_2 moves away from Obj_2, the wavefront converges, and the focal plane moves upward axially to Z = –100 µm. (b) When M_2 moves toward Obj_2, the wavefront diverges, and the focal plane moves downward axially to Z = 100 µm.

3.3 Performance of remote axial scan

The wavefront of the excitation beam changes as the mirror surface of the axial MEMS actuator M_2 moves in either direction away from the neutral position (Z_{M2} = 0 µm). When the mirror is 200 µm away from Obj_1 (Z_{M2} = –200 µm), the wavefront converges onto Obj_2, and the focal plane moves ~100 µm toward the tissue surface, Fig. 4(a). Similarly, when the

Optics EXPRESS

mirror moves closer to Obj_1 (Z_{M2} = 200 μm), the wavefront diverges, and the focal plane moves axially with greater depth into the tissue, Fig. 4(b).

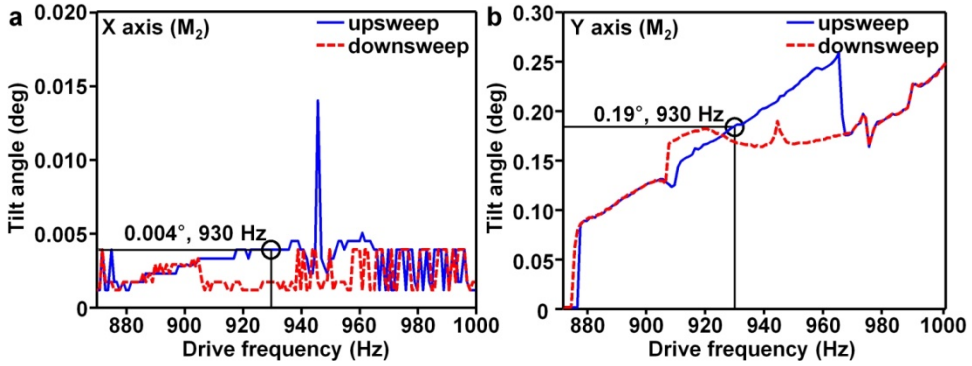

Fig. 5. Tilt angles of axial MEMS actuator. We measured (a) <0.004° and (b) and <0.19° in the X and Y axes, respectively, while translating a distance >400 μm at a drive frequency of 930 Hz.

The excitation beam may become miss-aligned if the mirror surface of M_2 tilts during translation. We used a position sensing detector (PSD) to measure the tilt angles about the X and Y axes during axial displacement over the range of drive frequencies. We measured a maximum tilt angle <0.004° in the X axis, Fig. 5(a), and <0.19° in the Y axis, Fig. 5(b), when the mirror is driven at 930 Hz. We also observed a rotational mode for this scanner at ~1200 Hz, which is out of the operating range of the actuator. These results show that we can achieve large axial scan displacements in the Z-axis with very small tilt angles in either the X or Y axes. Also, by properly designing the spring parameters, we can separate the frequency range between axial and rotational scan modes.

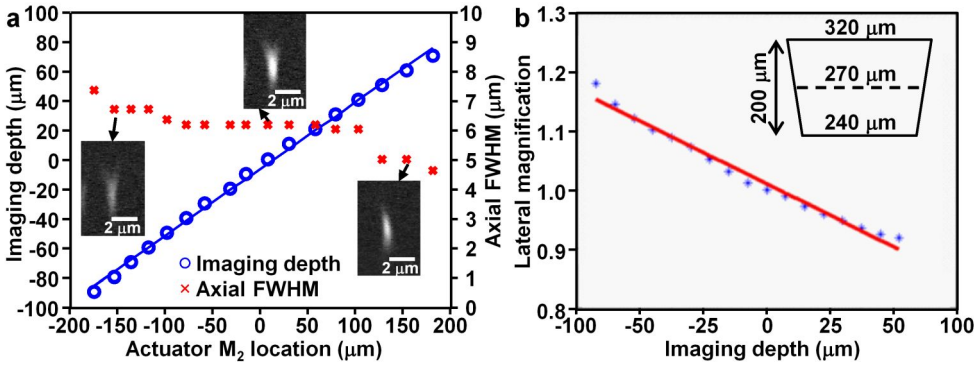

Fig. 6. Axial scan properties. (a) We found the position of M_2 and depth of the focus to have a linear relationship with slope of 0.45 and *P*-value = $2x10^{-20}$. Axial resolution defined by FWHM varies from 4.5 to 7 μm over scan range. (b) We found the lateral magnification to range from 0.9 to 1.2 over relevant imaging depths with slope of –0.0016 and *P*-value = $1.35x10^{-14}$.

We used a motorized stage to carefully adjust the position of M_2 while measuring the distance between Obj_2 and the focus, and found a linear relationship, Fig. 6(a). We found the axial resolution, defined by the FWHM, to vary from 4.5 to 7 μm over the scan range of M_2. With M_2 in the neutral position, we measured a lateral FOV of 270 × 270 $μm^2$. With translation of M_2, the lateral magnification decreases from ~1.2 to 0.9 as the focal plane moves from −100 μm to 100 μm from the neutral position, and the lateral FOV decreases from 320 μm to 240 μm, Fig. 6(b) inset. This difference results from a slight mismatch in the

Optics EXPRESS

optical parameters between Obj_1 and Obj_2, which are air and water immersion lenses, respectively.

Multiphoton excited fluorescence images of pollen grains were collected to compare vertical images generated by reconstructing a Z-stack of horizontal (XY) images with that collected directly in the vertical (XZ) plane using the axial beam scanning strategy. Images in the horizontal plane were collected over a FOV of 100 × 100 μm^2, Fig. 7(a). Horizontal images were collected while moving the specimen axially in 50 μm increments. A vertical image was extracted from the subsequent 3D reconstruction along the red line shown in Fig. 7(a), Fig. 7(b). By comparison, we collected an image in the vertical plane directly by axial translation of M_2, Fig. 7(c). Both sets of vertical images have a FOV of 100 × 50 μm^2. No significant differences can be appreciated in the resolution, intensity, or contrast between the vertical images collected using either approach.

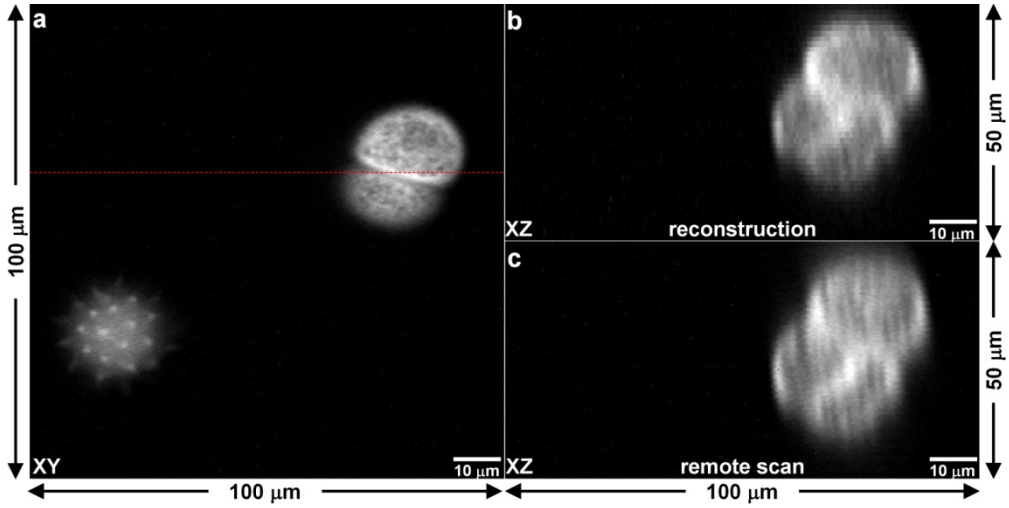

Fig. 7. Multiphoton excited fluorescence images of pollen grains. (a) Horizontal (XY) image using lateral MEMS scanner. (b) Vertical (XZ) image was reconstructed from series of horizontal images along plane marked by red line in a). (c) Vertical (XZ) image collected directly using MEMS actuator. Comparing panels b) and c), we calculated a Pearson's correlation coefficient of 0.897.

3.4 Imaging of epithelium

We further illustrate the axial scan capability of this system by collecting multiphoton excited fluorescence images from specimens of mouse colonic epithelium that express the optical reporter tdTomato ex vivo. A representative image obtained in the horizontal (XY) plane over a FOV of 270 × 270 μm^2 shows distinct crypt structures, Fig. 8(a). Hexagonally packed, circularly-shaped crypts (arrow) with uniform dimensions surrounding a central lumen (l) can be distinguished. Mucin-filled goblet cells (g) can be seen within cytoplasm (c) that produces uniform fluorescence. Individual inflammatory cells (arrowhead) can be identified in the lamina propria (lp). An image of the same epithelium was collected in the vertical (XZ) plane over a FOV of 270 × 200 μm^2, Fig. 8(b). The lumen (l) is now oriented vertically, and goblet (g) cells are seen distributed in the apical to basilar direction.

Optics EXPRESS

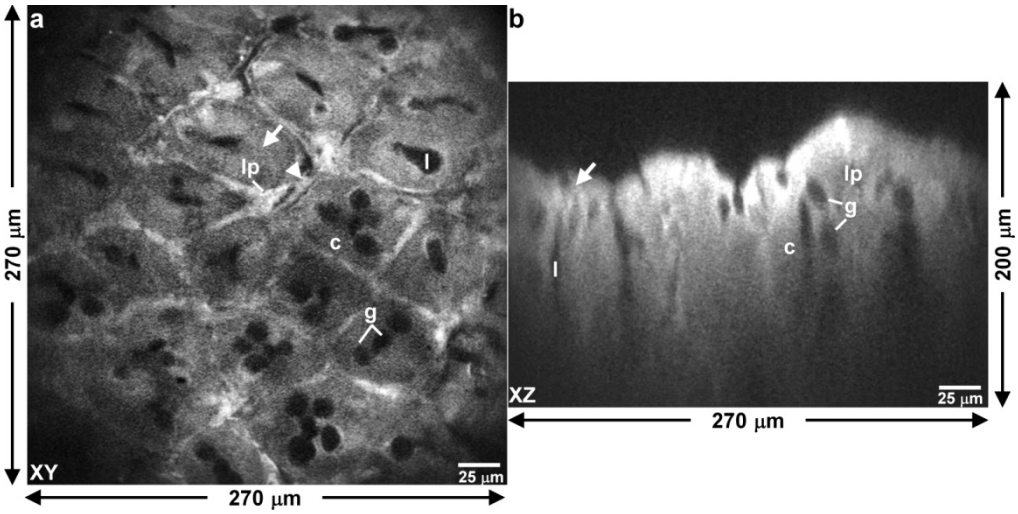

Fig. 8. Imaging of mouse colonic epithelium ex vivo. Representative multiphoton excited fluorescence images in (a) horizontal (XY) and (b) vertical (XZ) planes from specimen expressing tdTomato reveal crypt structures. Key: crypt (arrow), lumen (l), goblet cells (g), cytoplasm (c), inflammatory cells (arrowhead), lamina propria (lp).

4. Discussion

Here, we demonstrate a multiphoton microscope that uses a remote MEMS scanner and actuator to perform beam scanning in the axial direction so that optical sections can be collected in the vertical plane without moving either the optics or specimen. We collected vertical sections at 5 frames per sec. By comparison, conventional microscopes may take up to several minutes to acquire a stack of horizontal sections and then reconstruct vertical sections. Many biological processes associated with normal development and disease progression originate in the epithelium of hollow organs, such as colon, and extend downward in the vertical direction. Images in this plane can accurately localize the position of important biological phenomena relative to the tissue surface. Pathologists use this orientation to assess the depth of cancer invasion. These devices represent a promising alternative to large, bulky scanners and actuators found in conventional microscopes. We found these devices to be mechanically robust and highly reliable, and were able to fabricate at low cost with high yield.

We showed results to support multiphoton excited fluorescence images collected in the vertical plane using axial beam scanning to be equivalent to reconstructing a Z-stack of horizontal (XY) images acquired by moving the stage. We present fluorescence images collected from mouse colonic epithelium genetically engineered to express the optical reporter tdTomato with an imaging depth of ~200 μm at 5 frames per sec. These results demonstrate feasibility to collect vertical sections with an endomicroscope. We demonstrate a miniature scanner and actuator located remotely that images in either the horizontal or vertical plane. Scanning was performed separately in orthogonal directions to maximize the size of the mirror surface and to minimize higher order modes that may produce undesired motions that defocus the beam. We arranged the PBS and QWP with the excitation beam at normal incidence (rather than 45°) to use the full aperture of the lateral scan mirror M_1, Fig. 1(a). This configuration increases the beam diameter by a factor of 1.4, and introduces less scan induced distortions.

Despite our promising results, our study has several limitations. In the current configuration, the back aperture of the imaging objective (Obj_2) is slightly under filled, and in part explains why the theoretical diffraction limit for axial resolution of ~2 μm with a 0.9 NA objective was not achieved. This problem can be mitigated by increasing the diameter of the

Optics EXPRESS

lateral MEMS mirror to expand the width of the excitation beam. Our mirrors were designed to generate out-of-plane motion with a fully planar structure in resonance mode. Random access scanning can be achieved using dc microactuator designs that we are currently developing. In the vertical sections, we noticed a rapid reduction in signal with increased imaging depth as a result of tissue absorption and scattering over a long optical path. We can collect more signal at greater depths by modulating the laser to increase power with depth. An electro-optic modulator can be used to provide the speeds needed to match the fast axial scan rate of 465 Hz achieved by our MEMS actuator. Degradation in image resolution and reduced FOV can also be mitigated by a better match in the optical parameters between the air and water immersion objectives, Obj_1 and Obj_2, respectively [27].

There are a number of challenges that arise in adapting use of these MEMS devices in an instrument with an endoscopic form factor. The performance of a remote scan setup can be sensitive to optical misalignment and requires careful packaging. A polarization maintaining fiber with minimal dispersion is needed to deliver the ultra-fast laser pulses. Also, a miniature objective with high NA is needed to maximize photon flux. Previously, multiphoton endomicroscopes have been demonstrated by scanning a flexible optical fiber [28,29]. This approach images in the horizontal plane only, and not been developed for axial scanning so far. Here, we demonstrate use of a MEMS scanner and actuator that performs beam scanning to collect images in either the horizontal or vertical plane. The compact dimensions allow for future use in an endomicroscope.

5. Summary

Here, we demonstrate a remotely located MEMS actuator designed using the principle of parametric resonance that can translate >400 μm to produce vertical images with >200 μm depth. We measured a maximum lateral tilt angle for the actuator of <0.004° and <0.19° in the X and Y axes, respectively, over the scan range. We use a 2-dimensional MEMS mirror for lateral scanning, and collect images in either the horizontal or vertical plane at 5 frames per second. We found multiphoton excited fluorescence images of pollen grains collected in the vertical plane directly with the MEMS actuator to correlate with the reconstructed image from a stack of horizontal sections with a Pearson's coefficient of 0.897. We demonstrate ex vivo images of mouse colonic epithelium genetically engineered to express tdTomato. The compact size of the actuator and scanner allows for future use in an endomicroscope.

Funding

National Institutes of Health (NIH) R01 EB020644 and gift funds from Mary L. Petrovich.